MICROMETEOROIDS AND DEBRIS ON LDEF COMPARISON WITH MIR DATA

Jean-Claude Mandeville
Lucinda Berthoud
CERT-ONERA / DERTS
2, Avenue E.Belin, 31055 Toulouse Cedex (France)
Phone: (33) 61557117, Fax (33) 61557169

ABSTRACT

Part of the LDEF tray allocated to French experiments (FRECOPA) has been devoted to the study of dust particles. The tray was located on the face of LDEF directly opposed to the velocity vector. Crater size distributions have made possible the evaluation of the incident microparticle flux in the near-Earth environment. Comparisons are made with measurements obtained on the other faces of LDEF (tray clamps), on the leading edge (MAP) and with results of a similar experiment flown on the MIR space station.

The geometry of impact craters, depth in particular, provides useful information on the nature of impacting particles and the correlation of geometry with the chemical analysis of projectile remnants inside craters makes possible a discrimination between meteoroids and orbital debris. Emphasis has been laid on the size distribution of small craters in order to assess a cut-off in the distribution of particles in LEO. Special attention has been paid to the phenomenon of secondary impacts.

A comparison of flight data with current models of meteoroids and space debris shows a fair agreement for LDEF, except for the smallest particles : the possible contribution of orbital debris in GTO orbits to the LDEF trailing edge flux is discussed. For MIR, flight results show differences with current modelling: the possible enhancement of orbital debris could be the due to the contaminating presence of a permanently manned space station.

1. INTRODUCTION

The NASA Long Duration Exposure Facility (LDEF) has been retrieved after 2105 days in orbit. During its mission LDEF was stabilized with the long axis continually pointed toward the center of the earth, and surfaces perpendicular to this axis pointed at fixed angles with respect to the direction of orbital motion /1/.
The tray allocated to French experiments (FRECOPA) was located on the face of LDEF (B3) directly opposed to the velocity vector. Two passive experiments have been flown for the detection of microparticles. The first was composed of a set of thick metallic samples (Al, Au, Cu, W, Stainless Steel) and quartz surfaces; the second was composed of aluminium multilayer thin foil detectors. Detailed description of the hardware has been given elsewhere /2,3/.

The MIR Russian Space Station has been in orbit, between 350 and 425 km, since February 1986. The experiment, "Echantillons", was deployed outside the station during the Aragatz Mission in December 1988; it was retrieved 13 months later.
Dust detectors flown on MIR carried basically the same passive sensors as those on LDEF, with two sets of stacked thin foils (DMC) looking in two opposite directions, and an active capacitor type dust detector (DIC) /4/.

2. CRATER DISTRIBUTION AND MORPHOLOGY

Crater size distribution on the various targets enables, using laboratory calibration with solid particle accelerators, the evaluation of the incident microparticle flux. /5,6 7/.
It is important to remember that it is difficult to discriminate between craters of debris origin and those of meteoroid origin from a simple image of the crater. There are no specific characteristic forms for craters of different origins. However, crater morphology is determined by the interaction between particle and target. Particle and target properties will therefore have a major influence on crater parameters. Even when the particle has long since vapourised, craters may provide clues to its characteristics. Whilst pre-LDEF work concentrated on the interpretation of crater diameter (or spall and pit diameter for brittle targets), depth and depth to diameter ratio 'P/D', current crater morphology descriptions now also include crater cross-sectional profile, circularity and type of impact according to target thickness.

2.1. Crater diameter

Crater diameter has been shown in previous work to be dependent on many factors including particle size, density, velocity, impact angle and target properties, especially thickness /6,8/. In the case of semi-infinite space-exposed samples, the target properties are known and all the same. Therefore if the density and velocity of impacting particles are assumed, their sizes can be estimated. This size estimation is most rapidly found using one of the existing empirical equations developed from laboratory simulation tests. The crater diameters on LDEF examined in this work varied in size from 1.5 μm to 1070 μm and those for Mir varied from 0.5 to 300 μm. Calibration tests carried out recently /9/ showed that the Cour-Palais equation appeared the most suitable for converting micron-sized impacts on semi-infinite targets. Modelling values for velocities can be used with the Cour-Palais equation to convert the crater sizes mentioned above to particle sizes. This would give particle sizes of 0.5 μm to 395 μm for LDEF and 0.2 to 72 μm for Mir. Different crater measurement techniques create discrepancies when data is compared.

There can be up to a factor of 5 difference between the impact diameters formed on finite and semi-infinite targets for the same impactor size. This lead to only the 'thicker' foils on the Mir experiment being used to deduce crater size distributions. The observed crater size distributions for LDEF and Mir show two notable differences when compared to our model calculations and to McDonnell's experimental results /10/. The first is the 'bulge' in the distribution from crater diameter 5-50 μm on LDEF and from 1 to 10 μm on Mir. This is thought due either to secondary impacting or to the difference in scanning techniques. The second is the 'dip' in the distribution for craters < 5 μm on LDEF and < 1 μm on Mir. The dip could be explained by inadequate microscope resolution for Mir, but cannot be explained for LDEF leading and trailing edges, where it occurs for larger diameters (see figures 6,7 and 9).

2.2. Crater depth and crater depth to diameter ratio

The crater depth is examined here only as part of the P/D ratio. It is influenced by all the same parameters as the crater diameter. However, the hydrodynamic processes are different for crater depth and diameter formation. This can be seen experimentally for decreasing target thickness: the crater diameter remains constant up to and slightly beyond marginal perforation, whereas the crater depth increases. There is therefore no reason to believe that the depth and diameter will show the same parameter indices in their respective empirical equations. CTH calculations show that final crater depth is attained before final crater diameter /11/.The momentum enhancement effect is expected to slightly deepen craters for very high velocities due to the vapourisation of the target material. The depth is clearly affected by target material properties and thickness, particle shape and material properties.

The exact nature of parameters affecting the crater depth to diameter ratio have not yet been determined. Previous use of the ratio to deduce projectile density was based on the idea that the P/D depends only upon the density of projectile and target. As the density of the target was usually known the density of the projectile density was inferred from comparison with impact experiments. It was suggested that projectile density could provide a clue as to the composition of the particle. From experiments carried out in the laboratory we we have found that P/D is not influenced by impact velocity up to 14 km/s, when that velocity is above the target low stress bulk sound velocity. This is if agreement with Fechtig et al. Some research offers experimental evidence to the contrary /12,13/. Another complicating factor for P/D interpretation is the particle shape. The results from recent experiments show that fragmentary particles produce a wider variation in and a higher average of P/D compared to spherical particles /9/. The P/D is clearly a function of the position of the fragment when it strikes the target surface. The average P/D's found on spacecraft surfaces were above the expected 0.5-0.55.

For Mir, no P/D data could be extracted so far. But for LDEF, the P/D data we collected for a few hundred craters found on exposed surfaces may be useful for indicating particle densities.

For the trailing edge of LDEF (Figure 2), the craters of diameter < 100 μm were more uniformly spread over the P/D range and had a higher average P/D ratio than those of diameter > 100 μm. This implies that they were caused by particles of more widely varying densities/compositions with a higher average density than for larger particles. These large particles were more centered in the 0.5-0.6 range with small high and low density components. If the majority of impacts on the trailing edge are due to meteoroids, then the wide range of densities for smaller particles may reflect the heterogeneity of grain compositions. These different grains may come together to form a compact agglomerate, as seen in cosmic dust collections. The average density of such an agglomerate particle may well be around 2-3 g/cm^3, the value required to produce a P/D equal to 0.5-0.6 in the aluminium surfaces examined, as shown by test data.

On the leading edge of LDEF (Figure 3), an even wider spread of P/D was observed for the craters < 100 μm. The variety of densities implied by this spread could be explained by a wide variety of impactor types. For the smaller size range, debris are expected to dominate. Chemical analysis has already demonstrated the diversity of the debris family and this appears to be confirmed by the depth to diameter ratios. The larger craters were on average shallower and centered in 0.5-0.7 range. They are more likely to be due to meteoroids with lower average densities than debris. No particular 'families' of different impactors were discernible for these surfaces, such as those identified by Le Sergeant d'Hendecourt at 3 g/cm^3 and 8-9 g/cm^3 (corresponding to P/D's of 0.5 and 0.9 approx.) /14/.

One of the problems in the interpretation of these values is the vast range of compositions (and therefore densities) of impactors. It can be seen from the following that distinction between debris and meteoroid by P/D alone is not possible. Meteoroid and debris densities both cover the same range, resulting in similar P/D ratios:

P/D	(the target material is aluminium)
0.3-0.5 :	most likely to be meteoroids of low density. Could be paint flakes, (densities 0.5-1 g/cm^3)
0.5-0.6 :	likely to be aluminium or anything with a density similar to that of aluminium such as silicates including glass, stony meteoroids. (densities 2-3 g/cm^3)
0.6-0.7 :	some of the heavier elements and their alloys including titanium, silver etc. stony iron meteoroids (densities 4-5 g/cm^3).
0.7-1.0 :	most likely to be iron-based ie: either steel (debris) or iron meteoroids, or copper or copper alloy (densities 8-10 g/cm^3).

3. COMPARISON OF DATA WITH ESABASE MODELLING

The aim of the ESAbase meteoroid and debris application software /15/ is to assess particle flux and impact risk for a user-specified spacecraft geometry, mission parameters, spacecraft shielding, range of particles, particle flux models and damage equations. In this work the particle flux section of the code was exploited. The advantages of the code lie in its ability to describe the particle flux relative to an entire moving spacecraft (not just a single tumbling surface in space). Calculations take into account shielding effects, particle arrival direction and varying spacecraft attitude and pointing directions.

The Grün polynomial 1985 model /16/ is used for meteoroids (isotropic distribution) and the Kessler 1990 flux model is used for orbital debris; for more details see Anderson, ref. /17/. The velocity distribution relative to earth is taken from the Cour-Palais model /17/. Earth shielding and gravitational focussing are computed. For conversion from crater diameter (D) to particle diameter (d), or mass (m), the following equation is used (Cour-Palais) :

$$P / d = (5.24\, d^{0.056} / H^{0.25})\ (r_p/r_t)^{0.5}\ (V/c_t)^{0.667}$$

with : P : depth of crater and P/D = 0.56 for meteoroids and P/D = 0.63 for debris (measured)

d : diamater of particle in cm, r_p and r_t density of particle and density of target in g/cm^3

H : 90 (Brinell)

V : impact velocity in km/s, sound velocity in target : c_t= 5.4 km/s

3.1. LDEF flux model

The LDEF satellite is modelled by a 12-sided polygon. The mesh system allows identification of the flux on the different rows. The model includes the 8° offset towards row 10 with respect to the velocity vector which was observed on the return of the satellite.

ESAbase can be used to calculate the meteoroid and debris collision velocities for given spacecraft surfaces. Figure 4 shows the average calculated values for each different row on LDEF. The meteoroid velocities vary between 14.8 km/s and 22.8 km/s, velocity is 15.3 km/s for row 03 and 22.5 km/s for row 09. The debris velocities vary between 0 km/s (no flux) on row 03, and 11.5 km/s (rows 08 and 11), the debris velocity on row 09 is 10.7 km/s. ESAbase predicts a large difference in the debris flux for leading and trailing edges. All the rows towards the leading edge have an approximately similar debris flux; however, at row 05 (and its symmetric equivalent 01) the debris flux starts to fall off. By row 04, there is a factor 1000 difference and for 03 there is no debris flux at all. The modelled meteoroid flux does not show such a wide difference as the debris flux. There is a factor 10 difference between row 09 and row 03 for the meteoroids. The model predicts that the meteoroids will dominate the particle flux for crater diameters greater than 10 μm on rows 02, 03 and 04. See Figure 5.

We can perform a detailed comparison of model and observed data for row 09 by comparing crater size distributions with model data calculated by ESAbase. The model particle diameter and mass values were converted to crater diameters using the Cour-Palais empirical equation. Figure 6 shows that the experimental data lie between model predictions for meteoroids and debris for crater diameters less than 10 μm. For crater diameters larger than 10 μm, the experimental data approximately follow the total flux. From this we propose that the debris model is predicting too high a flux for small particles. This is consistent with findings by McDonnell and suggests that the micron end of the Kessler debris model needs modifying /18/.

On Figure 7, the crater size distributions found on FRECOPA surfaces is compared to the model for the trailing edge of LDEF. The occurrence of orbital debris in elliptical orbits could explain the difference between predicted and measured flux on the trailing edge. A cut-off in the distribution occurs for craters with a diameter smaller than 1 mm.

3.2. Mir flux model

The 1 m^2 Echantillons experiment module, with two sides AV and AR, was mounted on the conical part of the MIR station at 45° to the two symmetrical solar arrays.
According to information from CNES and from photographs, the longitudinal Y axis of the module was pointed at 45° to the sun and the Z axis at the Earth. However, due to certain orbital manoeuvres, the details of the orientation of the station are not known.
ESAbase calculates the impact velocity on the experimental surfaces for a given number of orbital points. Thus the variation of the impact velocity around the orbit can be monitored (Figure 8).
The debris velocity ranges between 0 and 13.5 km/s for the AV side (mean 7.6 km/s), 0 and 12.6 km/s for the AR side (mean 6.35 km/s). The meteoroid velocity ranges between 14.5 and 25.8 km/s (mean 19.2 km/s) for the AV side, and between 17.7 and 29.8 km/s for the AR side (mean 22.6 km/s).

ESAbase computes a meteoroid flux and a debris flux. These have both been converted to crater diameter using the Cour-Palais empirical equation and results are shown in Figure 9. The two crater size distributions can then be added together to give a total flux which might be seen on the experimental surface. It is now possible to compare the observed results for Mir and the ESAbase Mir model predictions. The model prediction underestimates the observed flux by a factor of around 6 for crater diameters between 1 and 50 μm.

Secondary impacts are common on some parts of MIR detectors. This is expected for complex large structures and can lead to an overestimate of actual flux. Hopefully the size distribution of secondaries is usually distinctive, with a large number of ovoid submicron craters. Discrimination is therefore usually possible. If the contribution of secondaries is removed, the flux of small particles on MIR orbit is still higher than expected by the models and similar to the flux on the leading edge of LDEF. The difference in altitude or inclination between Mir and LDEF cannot entirely explain the difference. It is possible that the environment of a permanently manned space station is populated by a large number of small, short-lived orbital debris.

4. ACKNOWLEDGEMENTS

The authors would like to express their thanks to Dr. F. Hörz and members of the Hypervelocity Gun Laboratory at NASA JSC in Houston and to Professor E. Grün at MPI in Heidelberg for carrying out acceleration tests, and to Professor J.A.M. McDonnell at the Univ. of Kent, Canterbury for LDEF MAP samples. This work was partly supported by a European Commission research grant under the 'Science' programme.

5. REFERENCES

1. A.S. Levine ed., *LDEF : 69 Months in Space*, NASA CP-3134 (1991), pp. 397-584.

2. J.C. Mandeville, AO138-1 and AO138-2 Experiments, in: *LDEF Mission 1 Experiments*, eds L.G. Clark, W.H. Kinard, D.J. Carter, J.L. Jones, NASA SP-473, (1984) p.121.

3. J.C. Mandeville and J.A.M. McDonnell, Micrometeoroid multiple foil penetration and particle recovery experiments on LDEF, in: *Solid Particles in the Solar System*, ed. I. Halliday and B.A. McIntosh, D.Reidel (1980) p.395.

4. J.C. Mandeville, Aragatz Mission Dust Collection Experiment, *Adv.Space Res.* 10, 3, 397, (1990).

5. J.C. Mandeville, Orbital debris and micrometeoroids : LDEF and MIR data, in: *Materials in a Space Environment,* Cepadues-Toulouse, (1992).

6. L. Berthoud and J.C. Mandeville, Empirical impact equations and marginal perforation, *Proceedings First European Conference on Space Debris,* ESA SD-01, (1993)

7. D. Humes, Large craters on the meteoroid and space debris impact experiment, in *LDEF - 69 Months in Space,* NASA CP-3134, (1991).

8. F.Hörz, R.P. Bernhard, T.H. See, D. Atkinson, M. Allbrooks, M and D SIG Progress Reeport : Laboratory simulations of LDEF impact features, in *LDEF - 69 Months in Space,* NASA CP-3134, (1991).

9. L.Berthoud, Micrometeoroids and orbital debris observed in low Earth orbit, Thesis, ENSAE, Toulouse, (1993).

10. J.A.M. McDonnell, Factors affecting the choice of foils for penetration experiments in space, in *Space Research X,* North Holland pub. (1970).

11 . A. Watts, D. Atkinson and S. Rieco, Dimensional scaling for impact cratering and perforation, *Report POD/Associates* , (1993).

12. H. Igelseder and E. Igenbergs, Crater morphology at impact velocities between 8 and 17 km/s, *Int. J. Impact Eng.,* vol.10,271-280, (1990).

13. J.Vedder and J.C. Mandeville, Microcraters formed in glass by projectiles of various densities, *JGR,* vol.79, 23, (1974).

14. L.B. Le Sergeant D'Hendecourt and Ph. Lamy, On the size distribution and physical properties of interplanetary dust grains, *Icarus* 43,350-372, (1980)

15. J. de Kruijf, ESABASE, A most versatile and flexible system engineering tool, *ESA BR-54,* (1988).

16. Grün E., Zook H. et al., Collisional balance of the meteoritic complex, Icarus 62, 244-272, (1985).

17. Anderson B.J., Meteoroid and orbital debris, NASA SP-30425, (1990).

18. J.A.M. McDonnell et al., Impact cratering from LDEF's 5.75 yr exposure, *Proc. Lunar Planet. Sci.* 22, 185-193, (1992)

Figure 1 : Crater depth to diameter ratio (P/D) against diameter (D) for clamps on various rows of LDEF.

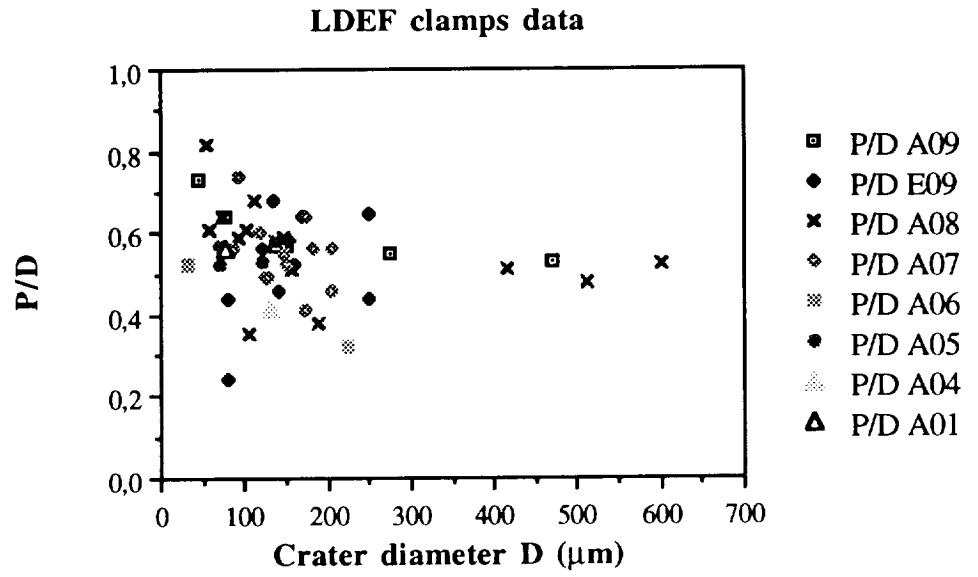

Figure 2 : Depth to diameter ratio (P/D) for craters on trailing edge (row03) of LDEF.

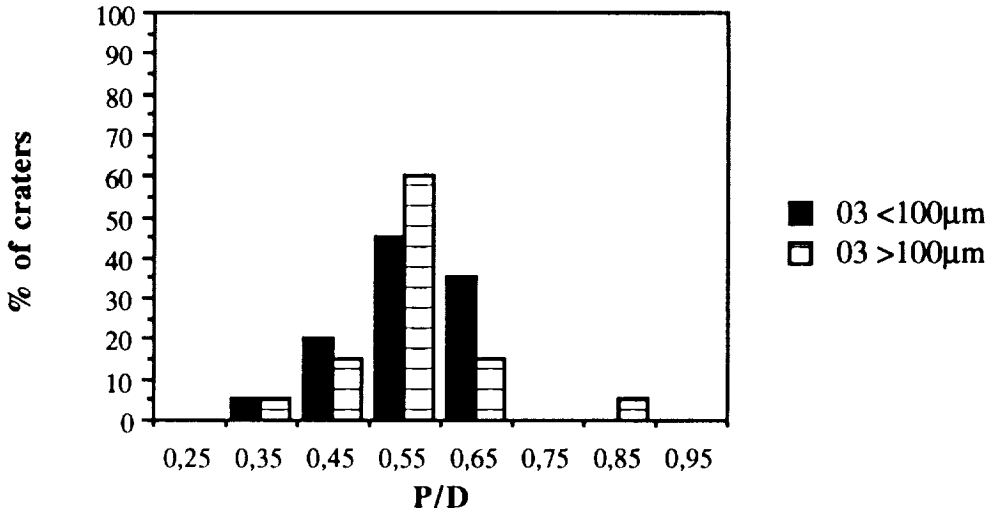

Figure 3: Depth to diameter ratio (P/D) measured for craters on leading edge (row 09) of LDEF.

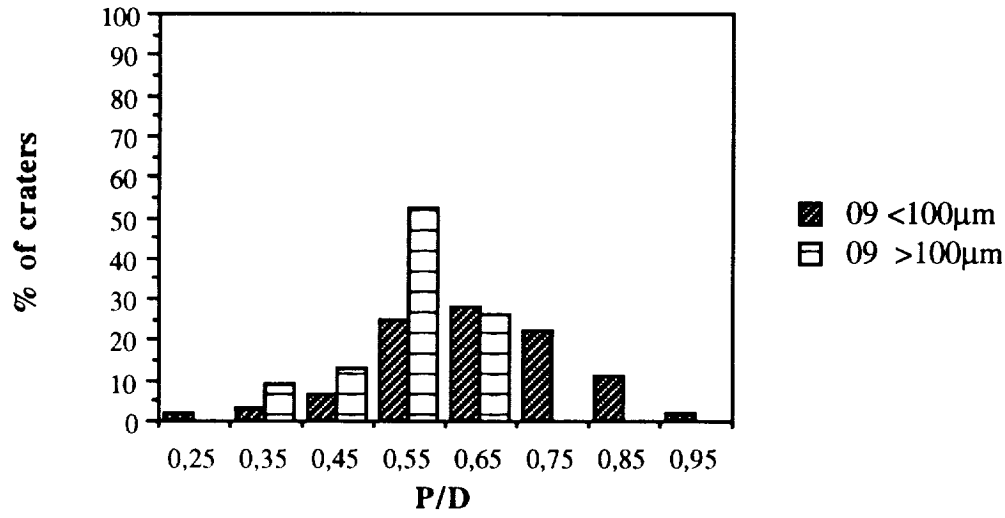

Figure 4. ESAbase calculated meteoroid and debris velocities for LDEF rows.

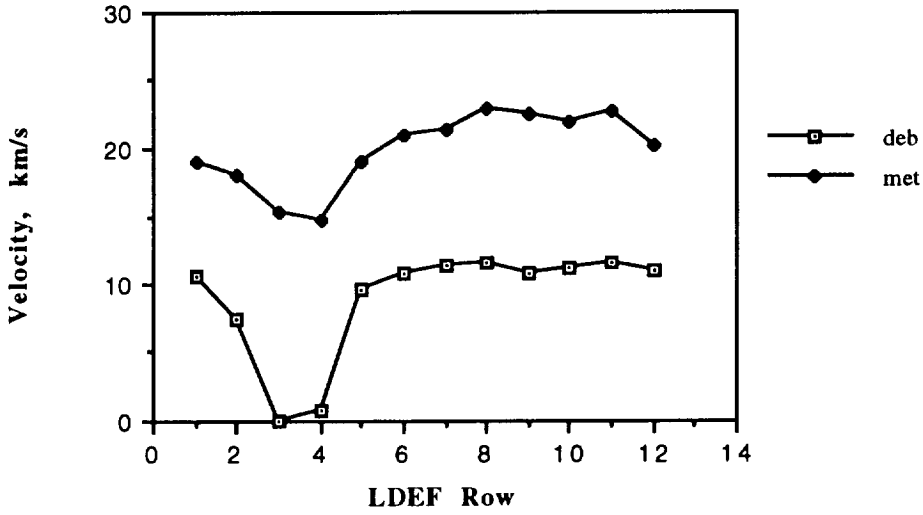

Figure 5 . ESAbase model predictions for meteoroids (modmet), debris (moddeb) and the sum of these (modtot) on all LDEF rows for craters with D > 10 μm (using Cour-Palais equation for the conversion crater diameter to particle diameter).

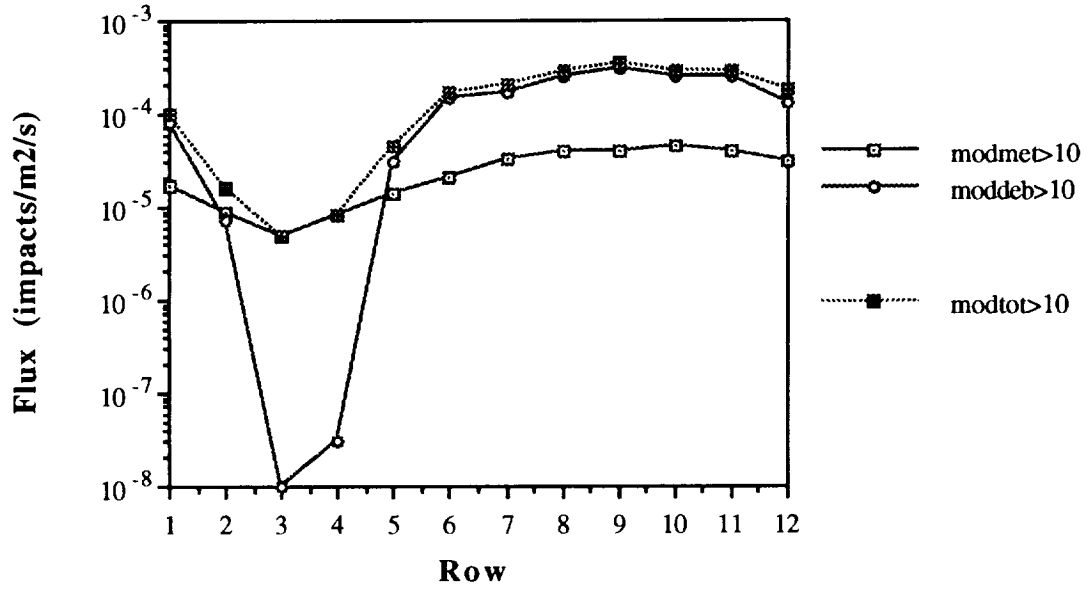

Figure 6 : ESAbase model predictions for debris (moddeb09) and meteoroids (modmet09) for the leading edge of LDEF compared to our experimental data (expt09).

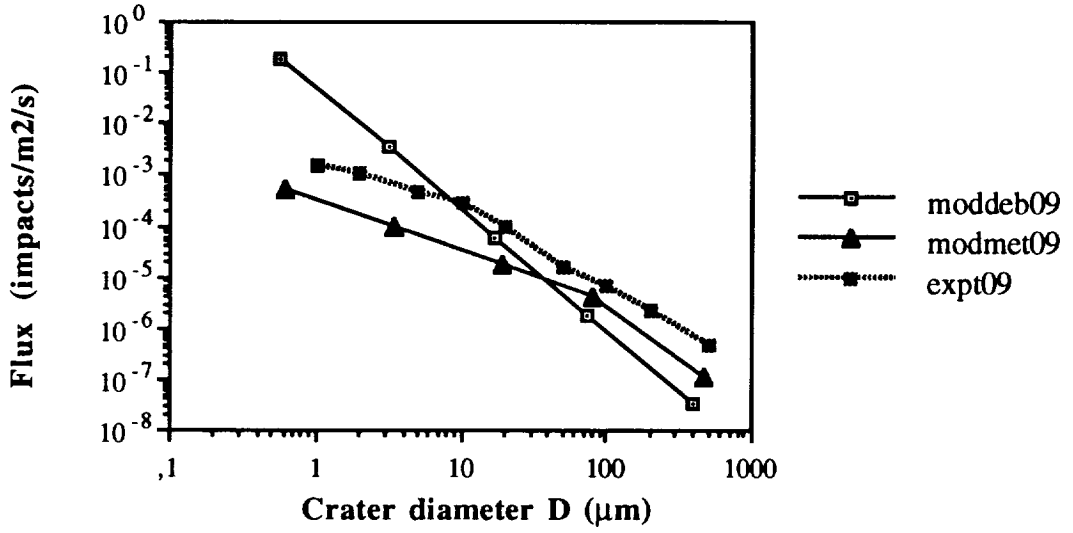

Figure 7 : ESAbase model of total flux for LDEF trailing edge (modmet03) compared to LDEF observed crater data (expt03).

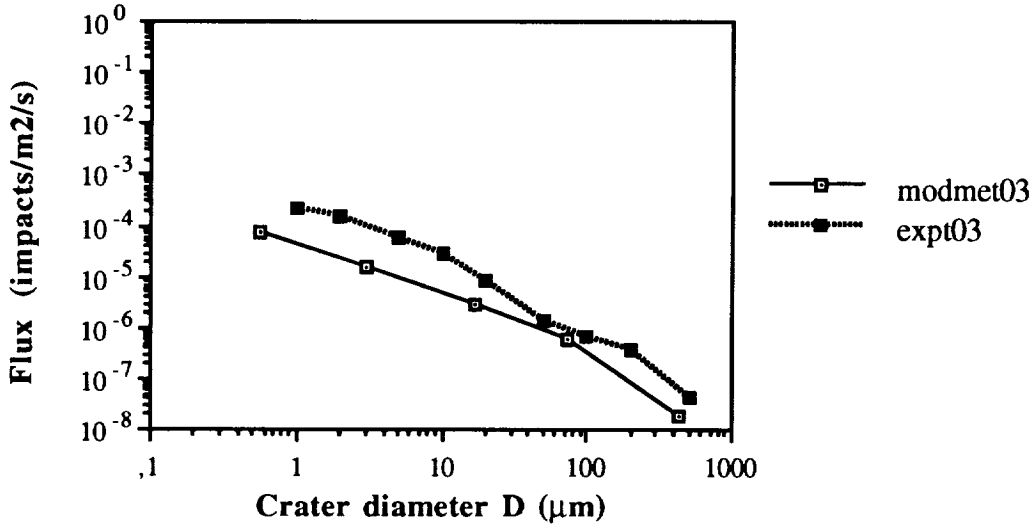

Figure 8 : Variation of meteoroid and debris velocities on Mir experiment around one orbit .

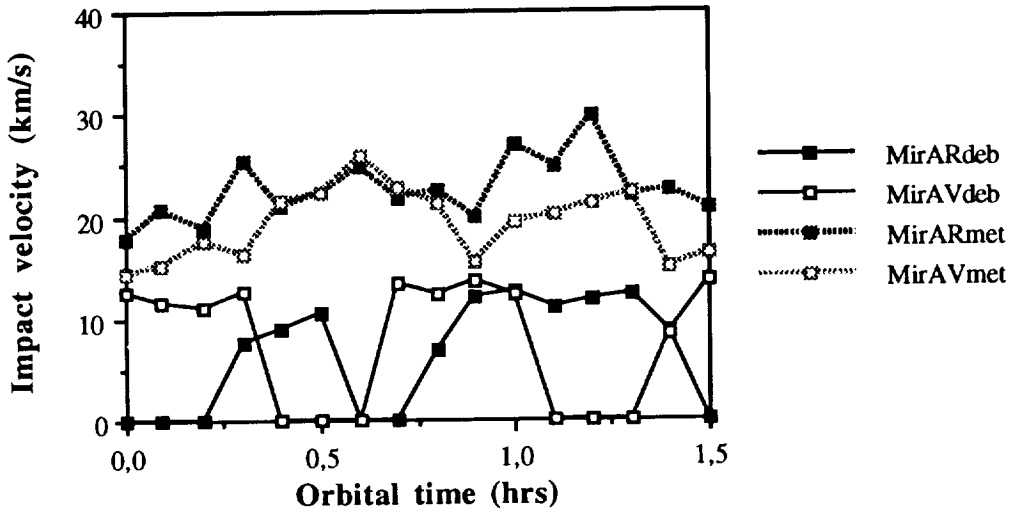

Figure 9 : ESAbase model of meteoroid (MirAVmet) and debris (MirAVdeb) flux compared to observed values (expAVthick) using Cour-Palais equation to convert d to D.